WILEY | Hindawi

Research Article

Fructus Aurantii Extracts Ameliorate Intestinal Inflammation and Regulate the Intestinal Barrier through Fc Epsilon RI Signaling Pathway

Sicong Liu [1] **Yongrui Bao** [1,2,3] **Shuai Wang** [1,2,3] **Tianjiao Li** [1,2,3] **Jiapeng Leng** [1] **Yi Zheng** [4] **Ying Meng** [1] **Ying Zheng** [1] **Bing Qi** [1] **Xi Luo** [1] **and Xiansheng Meng** [1,2,3]

[1]College of Pharmacy, Liaoning University of Traditional Chinese Medicine, Dalian 116600, China
[2]Liaoning Multi-Dimensional Analysis of Traditional Chinese Medicine Technical Innovation Center, Dalian 116600, China
[3]Liaoning Province Modern Traditional Chinese Medicine Research and Engineering Laboratory, Dalian 116600, China
[4]College of Integrated Chinese and Western Medicine, Liaoning University of Traditional Chinese Medicine,
 Shenyang 110847, China

Correspondence should be addressed to Xiansheng Meng; mxsvvv@163.com

Fructus Aurantii (FA) is the dry and immature fruit of *Citrus aurantium* L. and its rutaceous cultivars. FA has been widely used to treat digestive system diseases since ancient China, and it promotes gastrointestinal (GI) motility in functional dyspepsia (FD), but its potential therapeutic mechanisms remain unclear. We examined the effects of FA ethanol extracts in an iodoacetamide (IA)-induced FD rat model. Firstly, key FA therapy targets for FD were gathered using systematic pharmacology. Combined with systemic pharmacological analyses, plasma metabolomics based on UPLC-QTOF-MS were conducted. Then, MetaboAnalyst was used to jointly analyze systemic pharmacology targets and metabolomic metabolites to select key metabolic pathways. Finally, the key path is verified by experiments. FA exerted distinct therapeutic effects in anti-inflammation and promoting gastrointestinal motility in our IA-induced FD rat model. When compared with the model group, FA down-regulated the inflammatory factors interleukin 1β and tumor necrosis factor-α. At the same time, FA up-regulated tight junction proteins in the intestinal epithelial barrier. Through the integrated analysis of metabolomics and systemic pharmacology, we conducted experimental verification on Fc epsilon RI signaling pathway. When compared with the model group, FA down-regulatedphospho-mitogen activated protein kinase, phospho-extracellular signal regulated kinase1/2, myosin light chain kinase, and phospho-myosin regulatory light chain protein levels. Thus, FA ameliorated FD by regulating the Fc epsilon RI signaling pathway. Our integrated strategy identified underlying FA mechanisms toward FD treatment and provided a foundation for FA development as a clinical agent for FD.

1. Introduction

Functional dyspepsia (FD) is defined as the presence of symptoms thought to originate in the gastroduodenal region in the absence of any organic, systemic, or metabolic disease that readily explains the complaints [1]. It is one of the most common functional gastrointestinal disorders, affecting up to 16%–26% of the population [2], which increases year on year and seriously affects the quality of life of sufferers. In recent years, with a deepened knowledge of its pathophysiology, FD pathogenetic research has shifted from the stomach to the duodenum and focused on mild duodenal inflammation and intestinal barrier damage [3]. Growing evidence has shown that low-grade duodenal inflammation in FD was mainly based on the histological detection of a slightly but significant increased number of mucosal immune cells, mainly eosinophils and mast cells [4]. In a previous study, it has demonstrated that the intestinal barrier damage in FD patients found a correlation

between certain cell-to-cell adhesion proteins and low-grade inflammation [5]. Although the origin of this low-grade inflammation remains unidentified, it has been found that barrier dysfunction facilitates the passage of luminal antigens through the epithelium, thereby triggering an immune response. This, in turn, leads to low-grade inflammation, which contributes to the creation and persistence of gastrointestinal symptoms [6]. Currently, drug therapy is the major treatment for FD; while domperidone (Domp) and mosapride are effective treatments for the condition; their clinical use is restricted due to potential severe cardiovascular side effects [7]. Hence, safer and more efficacious FD treatments are required, and natural products may be an innovative source of such treatments. Presently, due to their benefits such as high compliance, remarkable curative effects, and fewer adverse effects, natural products are being used to treat and prevent FD.

Fructus Aurantii (Chinese name Zhiqiao) is the dried unripe fruit of *Citrus aurantium* L. that is collected from July. For a long time, the processed unripe fruits of bitter orange possesses homology of medicine and food characteristic, which is regarded to the health promotion effect in the digestive tract system. Since ancient times in China, Fructus Aurantii (FA) has been used for digestive system diseases. The "Supplementary Records of Famous Physicians" (the late Han Dynasty, approximately 220 A.D.) recorded that "FA eliminated flatulence and calmed the intestines and stomach." FA also relieves gastrointestinal syndrome induced by FD and exerts significant curative effects for the condition [8, 9]. FA has diverse pharmacological activities, including antidiabetic, antidepression, anticancer, antikidney stone formation, and cardiovascular protection [10–12]. Clinical trials and pharmacological studies have confirmed its effects for treating GI dysfunction by accelerating GI transport and gastric emptying [9, 13]. FA reportedly elevates gastric emptying rates, intestinal propulsion, and motilin and gastrin serum levels in rats [14]. Also, the pharmacological components of FA, such as narirutin, naringin, and hesperetin, reportedly exert anti-inflammatory effects by inhibiting the lipopolysaccharide-mediated activation of NF-κB and MAPKs [15, 16]. Through 5-H4R/cAMP pathway activation, naringin, hesperidin, and hesperetin regulate intestinal epithelial tight junction (TJ) proteins and intestinal flora, thereby improving GI function [16, 17]. Although many studies have confirmed the therapeutic efficacy of FA for FD, its effective constituents and related anti-FD mechanisms are unclear, which complicates its clinical application to modern medicine. Hence, identification of efficacious FA constituents and their mechanisms of action are warranted.

Metabolomics is an important drug research method, which can systematically detect the dynamic changes of small molecule metabolites in vivo [18, 19]. Given the complexity of multiple natural products constituents, it is difficult to screen for representative combinations of active constituents; the process is usually time-consuming, laborious, and leads to unsatisfactory results. Interestingly, metabolomics and natural products share similar system characteristics. Hence, metabolomics has been evaluated as the most common and effective method for the efficacy of natural products, comprehensively identifying and potentially explaining the molecular mechanisms underpinning

different diseases and relevant natural products treatments [20]. In 2007, based on the interactive information from diseases, genes, targets, and drugs [21], systematic pharmacology [22] was proposed as an effective data mining tool. Currently, many systematic pharmacology studies have been performed and successfully predicted associations between herbal products and certain disease-related targets [23–25].

In this study, metabolomics and systemic pharmacology were jointly applied to screen core signal pathways, and then experimental verification was conducted for the hub targets of the core pathway. Finally, a complete active herbal compound-target-pathway-biomarker network was constructed to explain the therapeutic efficacy of FA toward FD.

2. Materials and Methods

2.1. Materials and Reagents. FA (specimen number: 20210220, Quanjian, China) was identified as *Citrus aurantium* L. by Professor Zhang Hui, College of Pharmacy, Liaoning University of Traditional Chinese Medicine, Liaoning, China. Domp tablets (Lot. No. KJJOYG3) were supplied by Janssen, China. Standard reagents such as pentobarbital sodium (Merck, Germany), nobiletin, limonin, 3,4-dihydroxybenzaldehyde (purity ≥98%) were supplied by Weikeqi, China. Acetonitrile (LC-MS grade, Merck, Germany), methanol (LC-MS grade, Merck, Germany), and formic acid (LC-MS grade, Fisher, USA) were used. Enzyme-linked immunosorbent assays-tumor necrosis factor-α (TNF-α) (Lot: E-EL-R2856c, Elabscience, China) and interleukin-1β (IL-1β) (Lot: KE20005, Proteintech). PrimeScript™ RT reagent Kit (Lot. No. AT311, Transgen, China). Antibodies; Zonula occludens-1 (ZO-1), Occludin, Myosin light chain kinase (Mlck), and Myosin light chain2 (Mlc2) (Lot. No's. 21773-1-AP, 27260-1-AP, 10906-1-AP, and 21642-1-AP, respectively Proteintech, UK), Extracellular signal regulated kinase (Erk), Mitogen activated protein kinase (Mek), phospho-Mek (P-Mek), and phospho-Mlc2 (P-Mlc2) (Lot. No's. 4372S, 8727T, 9154S, and 3671T, respectively, Cell Signaling Technology, USA), P-Erk1/2 (Lot. No. 340767, Zenbio, China), and Iodoacetamide (IA) (Lot. No. 604E036, Solarbio, China).

2.2. FA Extract Preparation. The FA extraction method, comprising extraction solvents, methods, and times, was optimized in previous studies [26]. In our study, 100 g FA powder was added to 70% ethanol (1 : 10, w/v) boiled for 1 h and the process repeated three times. After decoction, the filtrates were merged and filtered by three layers of gauze. The filtrate was collected and concentrated to 0.27 g·mL^{-1} in the rotary evaporator. One ml of FA solution was diluted in 99 ml methanol and filtered using a 0.22 μm microporous membrane before qualitative analysis.

2.3. Qualitative Analysis of FA Active Ingredients. Qualitative analyses were performed using an Agilent 6550 precise mass quadrupole flight time instrument (Agilent Technology Co., Ltd.) using an Agilent pore shell SB-C18 column (100 × 2.1 mm, 2.7 μm) at 40°C. The mobile phase consisted of 0.1% formic aqueous solution (A) and

acetonitrile (B) over the following gradient: 5%–24% B at 0–9 min; 24%–43% B at 9–24 min; 43%–85% B at 24–33 min; 85%–100% B at 33–36 min. The flow rate was 0.4 ml/min and the injection volume was 1 μl. For MS detection, acquisition parameters were as follows: drying gas flow rate = 13 l/min; drying gas temperature = 250°C; nebulizer gas pressure = 45 psi; capillary voltage = 3500 V; fragmentor voltage = 125 V. The mass range was 50–1200 m/z. All samples were analyzed in negative and positive ion mode. Data were collected and processed using Agilent Mass Hunter software (version B.06.00).

2.4. Animals.
In order to minimize animal suffering, we provided the best care. The experimental procedures followed the Guide for the Care and Use of Laboratory Animals (United States National Institutes of Health Publication No. 85–23, revised 1986). This study was reviewed and approved by the Institutional Animal Care and Use Committee of the Liaoning University of Traditional Chinese Medicine (approval No.: 2019YS(DW)-33-01). Male Sprague Dawley rats (10 days old, 24 ± 3 g) were purchased from Liaoning Changsheng Biotechnology Co., Ltd, China. Rats were kept at 25°C ± 2°C in a 12 h/12 h light/dark cycle, with ad libitum access to food and water. The experiment was carried out as describing in literature [27]. Rat pups were then intragastrically administered 0.1% IA plus 2% sucrose at 0.2 ml/100 g once a day for 6 days, whereas control rats received 2% sucrose (0.2 ml/100 g) only. At 6 weeks, IA-treated rats underwent alternate-day fasting for 2 weeks, after which rats were randomized into three groups (n = 8/group) as follows: FD group (gavaged with an equivalent normal saline volume), FA group (gavage with 2 ml FA extract (2.7 g/kg crude drug according to the optimal dose based on the previous pharmacodynamics study of the research group [23])), and the Domp group (gavaged with 2 ml Domp solution (at 0.14 g/kg in water) once a day for two weeks). From the first day of IA administration to the day before euthanasia, rat mental state, weight, and food intake data were monitored on a weekly basis. Rats were fasted for 12 h before the last administration. Then, they were anesthetized with 1% pentobarbital sodium (40 mg/kg), and blood and duodenal tissue were rapidly collected. After that, animals were euthanized immediately via pentobarbital sodium intraperitoneal injection (100 mg/kg) [28]. For histopathology, 1 cm long duodenal tissue samples were fixed in 4% paraformaldehyde, while remaining samples were immersed in liquid nitrogen and stored at −80°C until required (Supplementary Material S1).

2.5. Exploring Gastric Emptying and Intestinal Propulsion.
After the last treatment, animals were fasted for 12 h. Rats had been fed with nutritious semisolid paste containing graphite powder (2 ml) by gavage. After 30 min, rats were humanely euthanized, and the abdominal cavity opened immediately. In the absence of obvious intra-abdominal abnormalities, pyloric orifice and gastric cardia ligation were performed, followed by whole stomach and small intestine removal. Thereafter, we weighed the whole stomach, then eliminated the stomach contents by immersing the stomach in 0.9% normal saline, and dried the stomach with sterile filter paper and weighed it. At the same time, we measured the distance the graphite powder moves from the pylorus and the length of the entire small intestine. Then, we evaluated gastrointestinal motility by gastric residual rate and intestinal propulsion rate (Supplementary Material S2).

2.6. Histopathological Examinations and Immunohistochemistry Analyses.
We embedded 4% paraformaldehyde-fixed duodenal tissue in paraffin, sectioned tissue into 4 μm slices, and hydrated and stained samples in hematoxylin and eosin (H & E) for microscopic analysis.

Following euthanasia, rat duodenal tissues were quickly isolated and washed in normal saline after removing attached tissue. Then, 1 cm duodenal biopsy specimens were fixed in 4% paraformaldehyde for 24 h, embedded in paraffin, sliced into 4 μm sections, stained in H & E and toluidine blue solution, and observed microscopically (Nikon Eclipse C1, Japan). Sections were incubated overnight at 4°C with primary antibodies for ZO-1 (1 : 1,000) and Occludin (1 : 400) and washed three times. After washing, a corresponding horseradish peroxidase (HRP)-labeled secondary antibody (1 : 300) was added to allow for a 50 min incubation period at room temperature. Then, after slightly drying, a 4′,6-diamidino-2-phenylindole solution was added to slides for 10 min at room temperature in the dark to stain nuclei. After washing, sections were dried slightly, mounted with antifluorescence quenching mounting agent, and observed under fluorescence microscopy. We captured 200x and 400x images which were quantitatively analyzed using Image J 8.0 (National Institutes of Health, MD, USA).

2.7. Inflammatory Cytokine ELISA.
For ELISA, plasma inflammatory biomarkers were detected using IL-1β and TNF-α kits as per manufacturer's instructions. Absorbance at 450 nm was measured using enzyme markers, standard curves plotted, and IL-1β and TNF-α levels determined.

2.8. Quantitative-Polymerase Chain Reaction (qPCR).
Total RNA was extracted using Trizol reagent according to manufacturer's instructions. cDNA was synthesized using TransScript OneStep gDNA removal and cDNA Synthesis Super Mix kits according to manufacturer's instructions. Subsequently, qPCR was conducted according to manufacturer's protocols under the following conditions: denaturation for 30 s at 94°C, followed by 40 cycles of 5 s at 94°C and 30 s at 60°C on a Real-time Thermal Cycler 5100 using a SYBR-Green master mix. All samples were normalized against GAPDH expression. Relative gene expression was analyzed using the $2^{-\Delta\Delta Ct}$ method. Primer sequences are shown in Table 1.

2.9. Western Blotting.
Total duodenum tissue proteins were extracted in RIPA lysis buffer (plus 1 mM PMSF and phosphatase inhibitors), and concentrations determined using a spectrophotometer (BioTeke ND5000, Beijing,

TABLE 1: Primer sequences of the genes used for Q-PCR.

Genes	Forward primer	Reverse primer
LYN	GAAGCCTGGACAATGGTGGTT	CCCATGGCTTCTGTGGTTTG
SYK	TGCCCATCCTGTGACTTGGT	CCTCCCGTTGGCTCATAGG
MEK	CAGTTGGAAGATACCCCATTCC	GAGGTCGGCTATCCATTCCAT
ERK	CTTTCCTCCGGCAAAATGAC	CCAGGTTGCTGTTCACCAGAA
GAPDH	CATGTTCGTCATGGGTGTGAA	GGCATGGACTGTGGTCATGAG

China). Proteins were separated using 10% sodium dodecyl sulfate polyacrylamide gel electrophoresis, transferred to polyvinylidene fluoride membranes, which were then blocked in 5% skimmed milk in Tris-buffered saline and 0.1% Tween 20 (TBST) for 1 h at 37°C, followed by overnight incubation with primary antibodies for ZO-1(1 : 2000), Occludin (1 : 2000), Mlck (1 : 2000), Mlc2 (1 : 2000), Erk (1 : 2000), Mek (1 : 1000), P-Mek (1 : 1000), P-Mlc2 (1 : 1000), P-Erk1/2 (1 : 500), and β-actin (1 : 3000) at 4°C. Next, membranes were washed in TBST, incubated with an antirabbit lgG antibody conjugated to HRP at 37°C for 1 h and washed in TSBT. Protein signals in membranes were observed using an enhanced chemiluminescence kit following manufacturer's instructions. Protein signal densities and immune response analyses were performed using the Tanon-5200 imaging system (Tanon Science and Technology Co. Ltd., Shanghai, China) and ImageJ software.

2.10. Metabolomics Profiling of Plasma Samples.
Plasma samples were also generated for LC/MS analysis by protein precipitation with methanol; $600 \, \mu$l cold methanol was added to $100 \, \mu$l plasma samples, vortexed for 60 s, and centrifuged at 12,000 rpm for 15 min at 4°C. Then, the supernatant was dried under nitrogen gas, and residues were redissolved in $30 \, \mu$l 50% methanol aqueous solution. We also prepared internal quality control (QC) samples by mixing $10 \, \mu$L of each test sample. All samples were maintained at 4°C during analyses. Mobile phase and gradient parameters were identical to aforementioned parameters (Section 2.3) and the injection volume was $3 \, \mu$l.

2.11. Systematic Pharmacology Analysis.
FA chemical constituents were imported into the TCMSP (https://lsp. nwu.edu.cn/index.php) database to filter active compounds through oral bioavailability (OB ≥ 30%) and drug-like properties (DL ≥ 0.18). Active compounds were imported into PharmMapper (https://www.lilabecust.cn/pharmmapper/index.html) and Swiss Target Prediction (https://www.swisstargetprediction.ch) databases to collect corresponding targets. FD-related target genes were obtained from DrugBank (https://www.drugbank.ca/), GeneCards (https://www.genecards.org/), OMIM (https://omim.org/), and DisGeNET (https://www.Disgenet.org/). Furthermore, we submitted the acquired target genes to STRING (https://STRING-db.org/) to recognize the functional protein association networks in accordance with calculation parameters and screening scores.

2.12. Joint-Pathway Analysis.
Joint-pathway analysis of differentially expressed metabolites with target proteins was performed using MetaboAnalyst 5.0 (https://www.metaboanalyst.ca) to derive insights on biological mechanisms associated with FD treatment. Then, an interaction network of herb-activecompound-hub target-pathway-biomarkers of FA treating FD was established. This network was visualized in Cytoscape (3.7.1) to show FD mechanisms.

2.13. Statistical Analysis.
Statistical analyses were performed in GraphPad Prism 8.0 (GraphPad, San Diego, CA, USA). Differences between two groups were assessed using one-way analysis of variance and presented as mean ± standard deviation. $P < 0.05$ value was considered statistically significant.

3. Results

3.1. LC-MS Analysis of FA and Compound Identification Using LC-MS Chromatograms.
Chemical constituents in FA extracts were analyzed by UPLC-QTOF-MS. Based on retention time, m/z, fragments from secondary MS, reference to the literature, and reference comparisons, 38 compounds were obtained. Total ion chromatograms are shown (Figure 1), while composition and other information are listed (Tables 2 and 3).

3.2. FA Attenuates IA-Induced FD Effects in Rats.
To examine the FD-attenuating effects of FA in rats, 10 day old animals were given IA, and their mental state, food intake, and weight data were monitored on a weekly basis (Figure 2(a)). When compared with the control group, weight gain in FD rats was significantly slow ($P < 0.01$) and food intake was significantly reduced ($P < 0.05$). After FA treatment, both weight gain ($P < 0.01$) and food intake ($P < 0.05$) in FD rats improved significantly. The weight gain and food intake of FA group were more than that of Domp group and close to that of control group (Figures 2(b) and 2(c)). FD rats exhibited markedly decreased GI motility, increased gastric residual rates ($P < 0.01$), and decreased intestinal propulsion rates ($P < 0.01$) when compared with controls. Also, when compared with the FD group, gastric residual rates ($P < 0.01$) decreased and intestinal propulsion rates ($P < 0.01$) increased in Domp and FA groups (Figure 2(k)). The effect of FA on promoting gastrointestinal motility in FD rats is similar to that of positive control drugs. A major pathological feature of FD is intestinal microinflammation. As expected, histopathological analyses showed the absence of
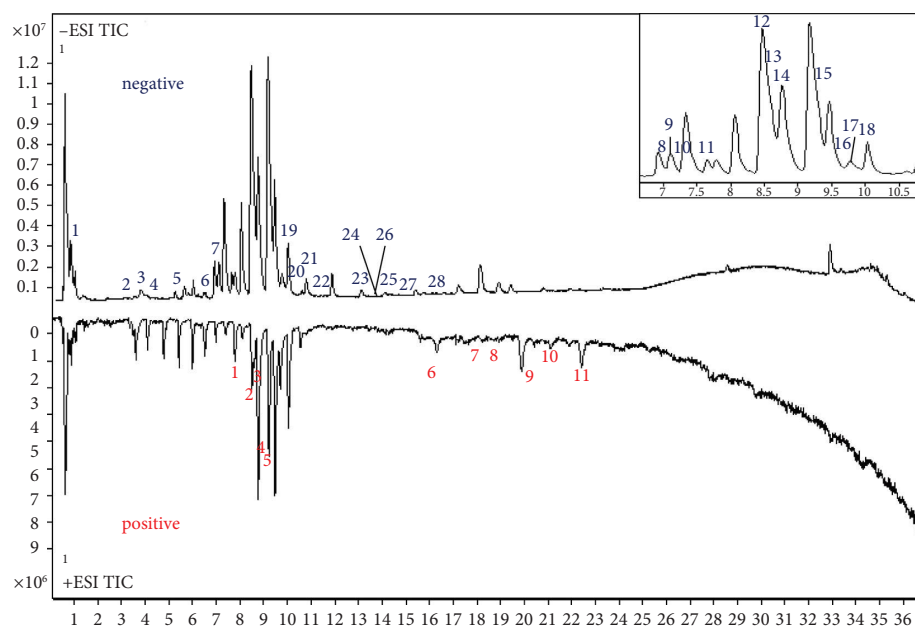
Figure 1: Total ion chromatograph of FA sample in negative and positive ion mode.

Table 2: Components of Fructus Aurantii in negative ion mode of MS.

No.	Systematic name	Molecular formula	Ion type	Precursor mass (m/z)	Found at mass (m/z)	Mass error (ppm)	Rt (min)	MS/MS fragmentations (m/z)
1	Citric acid	$C_6H_8O_7$	M-H	191.0197	191.0205	−4.05	0.943	111.0085
2	3,4-Dihydroxybenzaldehyde*	$C_7H_6O_3$	M-H	137.0244	137.0245	−0.6	3.142	108.0212
3	Chlorogenic acid	$C_{16}H_{18}O_9$	M-H	353.0878	353.0874	1.15	3.797	191.0564 127.0394
4	Caffeic acid	$C_9H_8O_4$	M-H	179.0350	179.0344	3.25	4.389	134.0370
5	Troxerutin	$C_{33}H_{42}O_{19}$	M + Cl	777.2014	777.2017	−0.35	5.699	579.1693 458.1178
6	Kaempferol-3-rutinoside*	$C_{27}H_{30}O_{15}$	M-H	593.1512	593.1508	0.66	6.756	271.0614 286.0479 151.0021
7	Eriocitrin*	$C_{27}H_{32}O_{15}$	M-H	595.1668	595.1672	−0.6	6.914	151.0039 135.0454
8	Rutin	$C_{27}H_{30}O_{16}$	M-H	609.1461	609.1462	−0.15	7.075	300.0207 271.0243 151.0020
9	Limonin-7-O-beta-D-glucoside	$C_{32}H_{42}O_{14}$	M-H	649.2502	649.2505	−0.49	7.137	606.2619 444.2106 228.1473
10	Neoeriocitrin	$C_{27}H_{32}O_{15}$	M-H	595.1668	595.1673	−0.77	7.187	460.1135 151.0041 135.0455
11	Cynaroside*	$C_{21}H_{20}O_{11}$	M-H	447.0923	447.0927	1.31	7.651	285.0387 119.0501
12	Narirutin*	$C_{27}H_{32}O_{14}$	M-H	579.1719	579.1726	−1.16	8.48	151.0042 272.0653
13	Naringin*	$C_{27}H_{32}O_{14}$	M-H	579.1719	579.1726	−0.29	8.592	460.1190 272.0649 151.0038 119.0501

Table 2: Continued.

No.	Systematic name	Molecular formula	Ion type	Precursor mass (m/z)	Found at mass (m/z)	Mass error (ppm)	Rt (min)	MS/MS fragmentations (m/z)
14	Rhoifolin*	$C_{27}H_{30}O_{14}$	M-H	577.1563	577.1562	0.14	8.737	459.1160 271.0618 269.0455 151.0040 119.0503
15	Hesperidin*	$C_{28}H_{34}O_{15}$	M-H	609.1825	609.1826	−0.17	9.376	302.0751
16	Nomilin glycosides	$C_{34}H_{46}O_{15}$	M-H	693.2764	693.2768	−0.59	9.761	566.2677
17	Heterophyllin	$C_{27}H_{32}O_{14}$	M-H	579.1719	579.1726	−0.29	9.936	272.0647 151.0042
18	Milinate-17-β-d-glucoside	$C_{34}H_{48}O_{16}$	M-H	711.2870	711.2866	0.5	9.969	652.2688 608.2782
19	Nominate-17-β-d-glucoside	$C_{34}H_{48}O_{16}$	M-H	711.2870	711.2868	0.22	10.081	652.2658 608.2783
20	Kaempferitrin	$C_{27}H_{30}O_{14}$	M-H	577.1563	577.1562	0.14	10.528	269.0449 151.0034
21	Poncirin*	$C_{28}H_{34}O_{14}$	M-H	593.1876	593.1864	1.99	11.424	286.0805 151.0053 107.0131
22	Quercetin	$C_{15}H_{10}O_7$	M-H	301.0354	301.0347	2.25	11.44	121.0292 151.0038
23	Apigenin*	$C_{15}H_{10}O_5$	M-H	269.0455	269.0458	−0.94	13.645	119.0506
24	6′,7′-Dihydroxybergamottin	$C_{21}H_{24}O_6$	M-H	371.1500	371.1497	0.84	14.109	254.0579 225.0557
25	Hesperetin*	$C_{16}H_{14}O_6$	M-H	301.0718	301.0717	0.21	14.317	286.0393 151.0039 134.0384
26	Diosmetin*	$C_{16}H_{12}O_6$	M-H	299.0561	299.0558	1.04	14.333	284.0323
27	6′,7′-Dioxy bergamot	$C_{21}H_{24}O_6$	M-H	371.1500	371.1498	0.57	14.669	225.0553
28	Pine oleic acid	$C_{18}H_{34}O_5$	M-H	329.2333	329.2334	−0.16	16.012	171.1014 139.1131

apparent histopathological morphology in control animals, while in FD animals, duodenal mucosa exhibited defects and inflammatory cell infiltration. After FA and Domp administration, histopathology was improved to varying degrees (Figure 2(d)).

3.3. FA Ameliorates Low-Grade Duodenal Inflammation and Repairs Damaged Intestinal Barriers in FD Rats.

Impaired duodenal integrity and low-grade inflammation are major pathological characteristics in FD [29]. When compared with controls, inflammatory cytokine IL-1β and TNF-α plasma levels significantly increased in the FD group ($P < 0.01$). After FA administration, these plasma levels were significantly reduced ($P < 0.05$) (Figures 2(f) and 2(g)). Intestinal barrier function is dependent on adjacent cell connections via junctional complexes at cell-cell contact sites and consists of tight junction, adherens junctions, and desmosomes [30]. TJ proteins include ZO-1 and occludin; ZO-1 connects to the transmembrane protein occludin and other cytoplasmic components, with key roles in TJ biology [31]. We observed that ZO-1 and occludin protein expression levels in the FD group had decreased ($P < 0.05$) when compared with controls, but the level of FA groups is increased ($P < 0.05$, $P < 0.01$) (Figures 2(e), 2(g)–2(i), and 2(l)).

3.4. Systematic Pharmacology Analysis.

Of the 38 compounds in FA extracts, 29 active substances were screened through OB and DL. By inputting these compounds into target databases, 1,018 FA targets were obtained. By gathering FD-related targets from disease databases, 1,207 FD targets were acquired (Figure 3(a)). After interactive analysis of component and disease targets, 252 putative targets underlying anti-FD mechanisms mediated by FA extracts were obtained (Figure 3(b)). Thereafter, these intersected genes were imported in STRING database for constructing the protein-protein interaction (PPI) network and for obtaining PPI networks relations (Figure 3(c)). Then, we constructed a connection diagram of the potential target related pathways of FA potential material basis based on systematic pharmacological analysis (Figure 3(d)).

3.5. Metabolomics Analysis.

Metabolic plasma sample profiles, generated by UPLC-QTOF-MS, were used to evaluate metabolomic alterations in study rats. Our PCA score chart showed a distinct separation between FD and control groups. Importantly, QC samples were highly clustered, indicating good instrument-based stability (Figure 4(a)). Additionally, 10 ions were extracted from basic QC sample peak intensity chromatograms for method validation. The RSDs of these 10 ions were in the 0.0981%–2.8325% region.

TABLE 3: Components of Fructus Aurantii in positive ion mode of MS.

No	Systematic name	Molecular formula	Ion type	Precursor mass (m/z)	Found at mass (m/z)	Mass error (ppm)	Rt (min)	MS/MS fragmentations (m/z)
1	1,8,15,22,29-Pentaaza-cyclopentatriacontane	$C_{30}H_{55}N_5O_5$	M + H	566.4276	566.4251	4.41	7.881	548.4097 453.3434 435.3287 153.0173
2	Naringenin chalcone	$C_{15}H_{12}O_5$	M + H	273.0757	273.0749	3.11	8.503	147.0436 119.0485 153.0167
3	Naringenin*	$C_{15}H_{12}O_5$	M + H	273.0757	273.0746	4.21	8.648	119.0488 147.0435 111.0065
4	Hesperidin	$C_{28}H_{34}O_{15}$	M + Na	633.179	633.1779	1.72	9.27	548.4097 453.3434 435.3287 311.0987
5	Neohesperidin*	$C_{28}H_{34}O_{16}$	M + Na	633.179	633.1777	1.41	9.382	487.1204 331.0999 185.0422 131.0489
6	Meranzin	$C_{15}H_{16}O_4$	M + H	261.1121	261.1112	3.58	16.387	189.0544 103.0542
7	Limonin*	$C_{26}H_{30}O_8$	M + H	471.2013	471.1996	3.71	18.177	425.1991 161.0584
8	3′,4′,7,8-Tetramethoxyflavone	$C_{19}H_{18}O_6$	M + Na	365.0996	365.0978	4.82	18.608	335.0486 373.0893 327.0817
9	Nobiletin*	$C_{21}H_{22}O_8$	M + H	403.1387	403.137	4.33	20.08	358.0711 345.1018 387.0936 211.0228
10	3′,4′,3,5,6,7,8-Heptamethoxyflavone	$C_{22}H_{24}O_9$	M + H	433.1493	433.1475	4.18	21.311	403.1987 385.0965 343.0791
11	Tangeretin*	$C_{20}H_{20}O_7$	M + H	373.1282	373.1266	4.23	22.43	300.0616 271.0591 211.0226

*Identified by comparing with the standards.

(a)

(b)

(c)
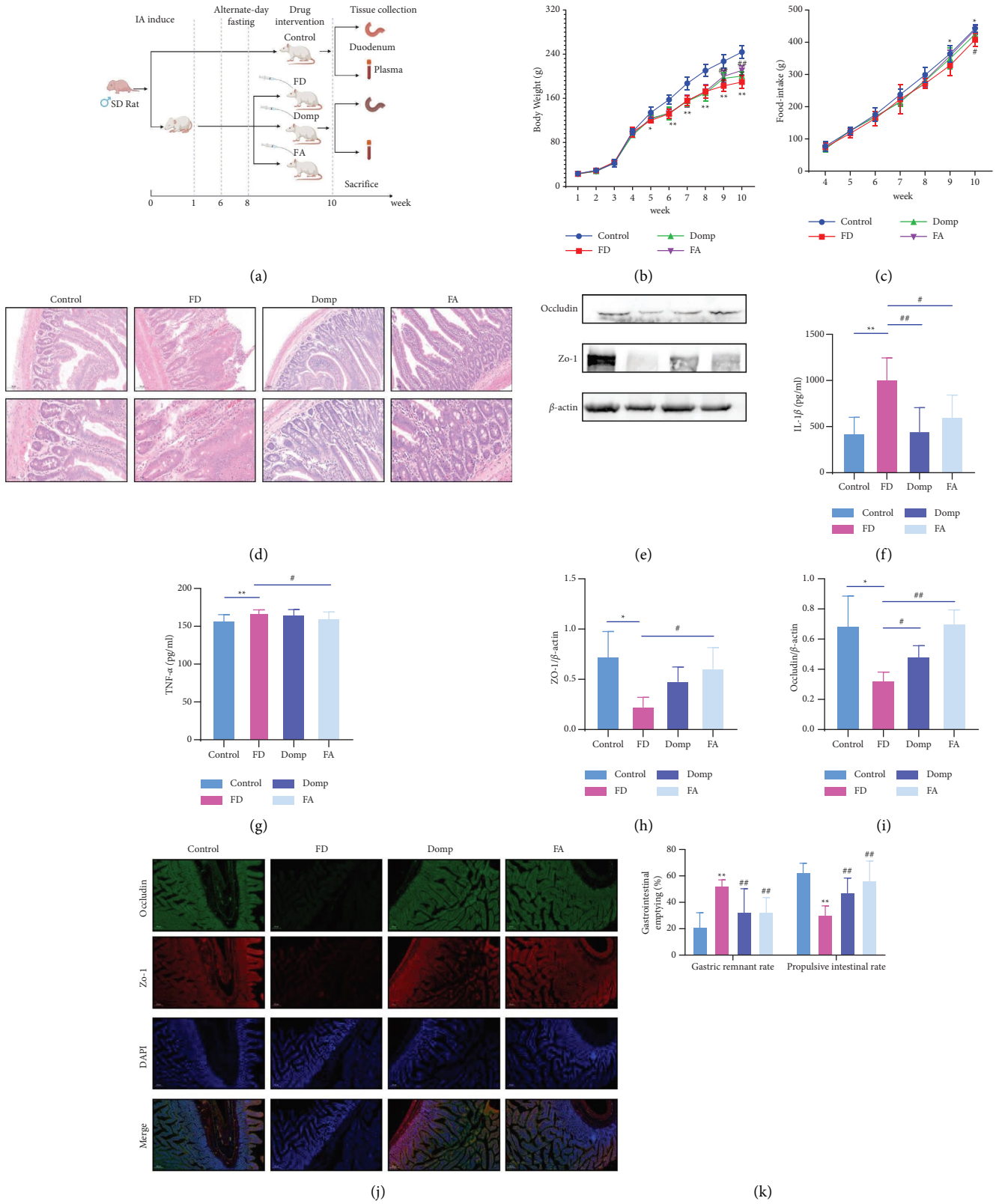
(d)

(e)
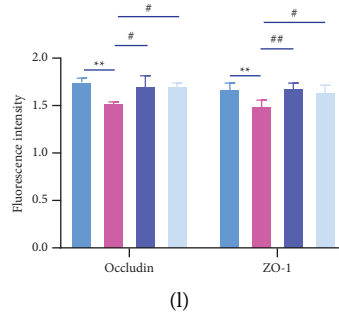
(f)

(g)

(h)

(i)

(j)

(k)

Figure 2: Continued.

(l)

FIGURE 2: FA alleviate IA-induced FD in rat. (a) Schematic diagram of the experimental process (created with Biorender.com). (b) Weight gain ($n = 8$). (c) Food intake ($n = 8$). (d) Representative images of duodenum pathologic damages with H & E staining, (scar bars: 100 μm, 200 μm). (e) Representative images of ZO-1 and occludin. (f) Detection of plasma IL-1β in rat of each group. (g) Detection of plasma TNF-α in rat of each group. (h) ZO-1 protein expressions ($n = 3$). (i) Occludin protein expressions ($n = 3$). (j) Immunofluorescence staining demonstrating the localization of ZO-1, occludin (scar bars:200 μm). (k) Gastrointestinal motility of rats in each group ($n = 8$). (l) The intensity of ZO-1 and occludin was determined by immunofluorescence ($n = 3$). Values are presented as the means ± SD. $^{*}P < 0.05$ and $^{**}P < 0.01$ were compared with the control group. $^{\#}P < 0.05$ and $^{\#\#}P < 0.01$ were compared with the FD group.
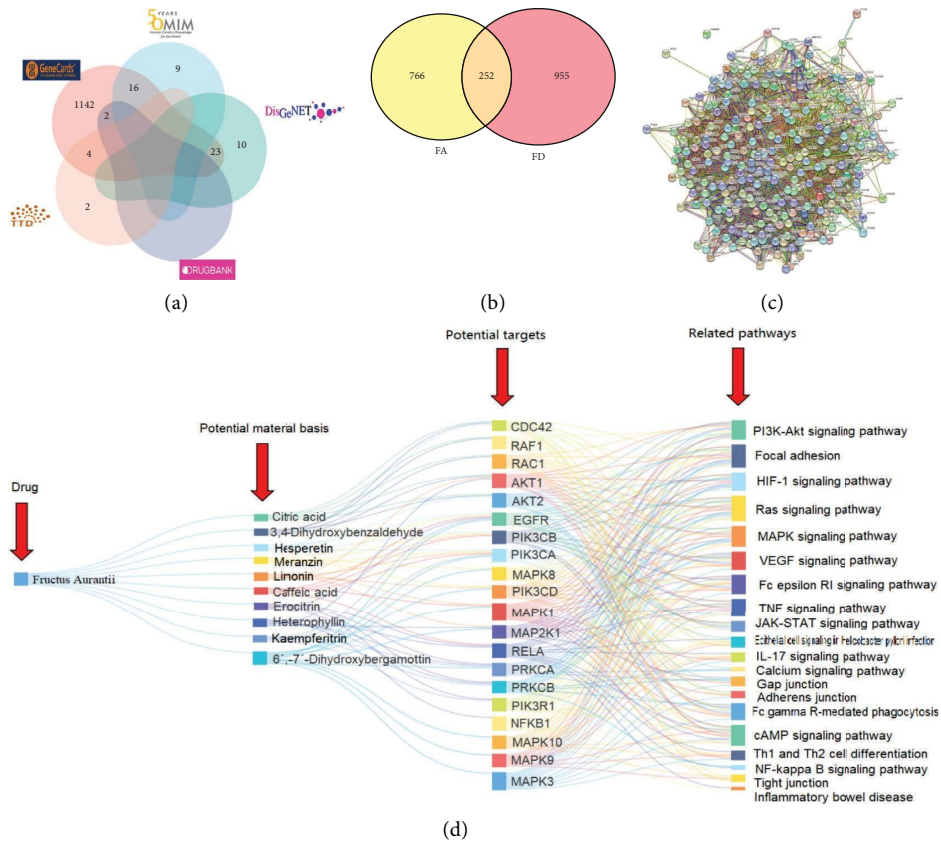

(a)

(b)

(c)

(d)

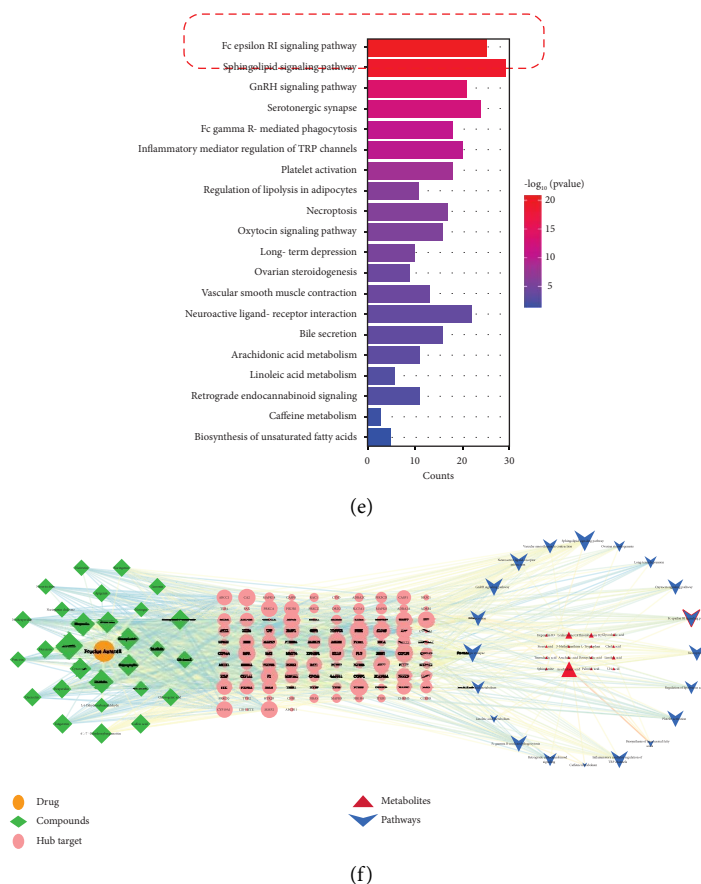FIGURE 3: Continued.

(e)

(f)

FIGURE 3: Systematic pharmacology analysis. (a) Venn diagram of targets number in FD database. (b) Venn diagram of intersection targets of FD and FA. (c) Protein-protein interaction network of hub targets. (d) Connection diagram of FA-potential material basis-potentialtargets-related pathways of systematic pharmacology analysis. (e) Joint pathway analysis of biomarkers and target disturbed by FA. (f) Active compound-target-biomarker-pathway network (the red line circles the experimental validation pathway).

To further identify different metabolites, we used supervised mode OPLS-DA (Figures 4(b) and 4(c)) to reduce the effects of intragroup differences on classification, thus maximizing separation between groups. To test the OPLS-DA model validity, a 200-permutation test was applied. All Q^2 values on the left were <those on the right. The intersection value between the Q^2 regression line and vertical axis was <0 (Figures 4(e) and 4(f)). This result ($Q^2 = 0.918$) showed the model was valid and no over-fitting had occurred in OPLS-DA models. Therefore, all OPLS-DA scores plots (Figures 4(b) and 4(c)) showed that control and FA groups were separated from the FD group. The S-plots of OPLS-DA revealed a variety of metabolites (Figures 4(h) and 4(i)).

3.6. Identification and Analysis of Endogenous Metabolites. Endogenous metabolites were identified according to VIP >1.0 and T-Test ($P < 0.05$) values. In total, 54 different metabolites were identified based on secondary spectrum information, and the HMDB database was where 30 metabolites were up-regulated and 24 metabolites down-regulated. To further clarify the distribution of the 54 differential metabolites in different rat groups, unsupervised clustering was performed using hierarchical cluster heat map

analysis. As shown (Figure 4(g)), model and control groups were separated into different clusters, while FA and control groups were gathered in the same cluster, suggesting FA had ameliorated the metabolic FD disorder. Metabolites were then introduced into the MetaboAnalyst program to investigate the metabolic effects of FA in FD rats. Metabolic pathways with an impact value >0.1 were related to the therapeutic effects of FA on FD. Our results showed that FA affected FD via different pathways, including linoleic acid, arachidonic acid, sphingolipid, tryptophan, pyrimidine, and purine metabolism, and also the pentose phosphate pathway, primary bile acid biosynthesis, glycerophospholipid metabolism, fatty acid biosynthesis, valine, leucine, and isoleucine degradation (Figure 4(d)) (Supplementary Material S3 and S5)

3.7. Joint Pathway Analysis of Targets and Metabolites. To explore key metabolic pathways, joint pathway analyses were performed on the 54 differential metabolites and 252 targets using MetaboAnalyst 5.0. As shown (Figure 3(e)), the Fc epsilon RI signaling pathway was concurrently rich in network pharmacology targets and metabolomics differential metabolites. Based on the number of targets in network
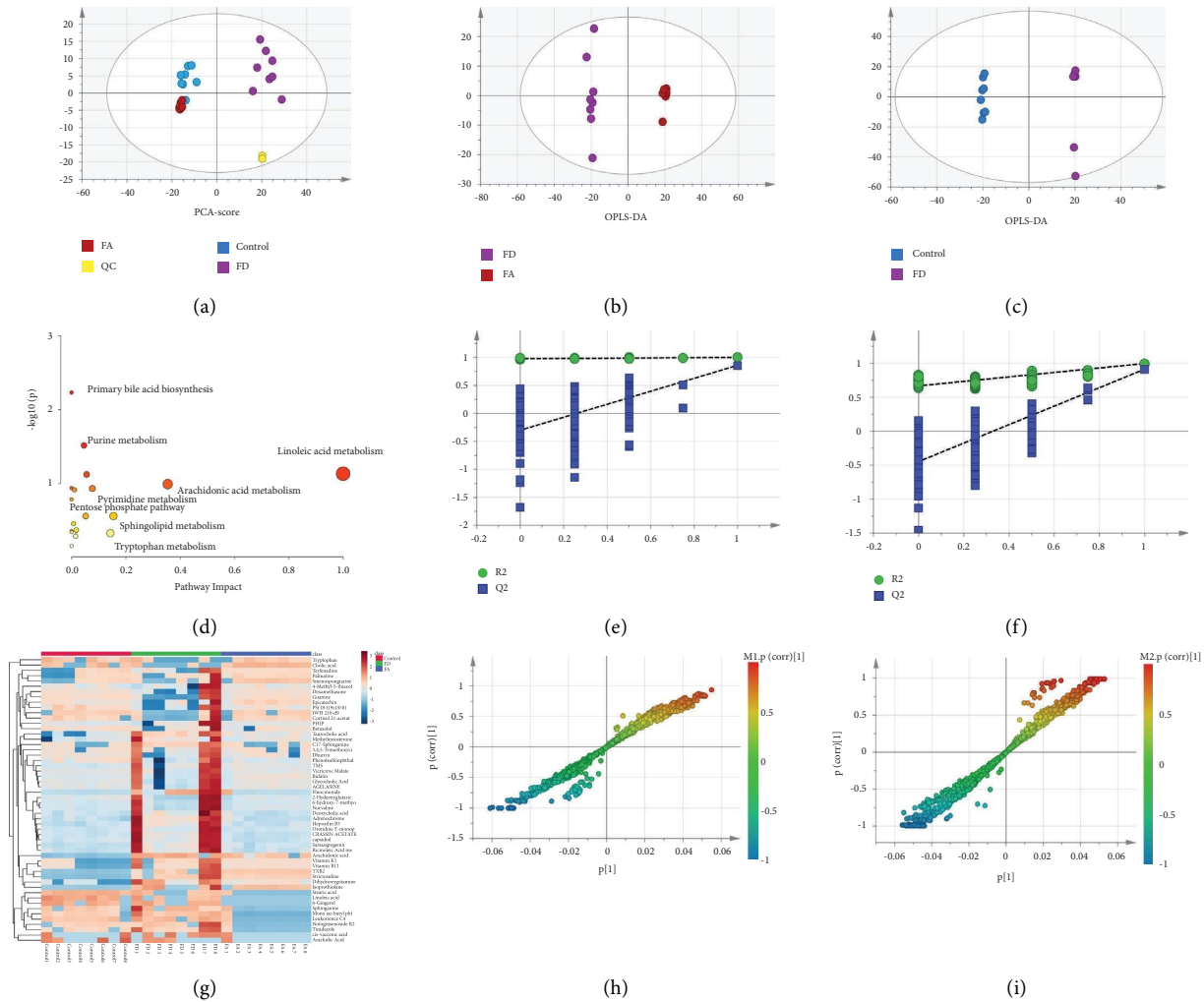
FIGURE 4: Systems' analysis of the metabolomic alterations in each group ($n = 8$). (a) PCA score plot in each group. (b) OPLS-DA score plot between control and FD ($Y2 = 0.995$ and $Q2 = 0.851$). (c) OPLS-DA score plot between FA and FD ($Y2 = 0.987$ and $Q2 = 0.918$). (d) Metabolic pathway analysis of different metabolites by metaboanalyst 5.0. (e) Validation diagram of the OPLS-DA model between control and FD. (f) Validation diagram of OPLS-DA model between FA and FD. (g) The heat map of metabolites in each group. Red means up-regulation, blue means down-regulation. (h) S-plot of OPLS-DA between control and FD. (i) S-plot of OPLS-DA between FA and FD.

pharmacological pathways, Fc epsilon RI signaling was selected for further experimental verification. Combining systemic pharmacology and metabolomics, we established a complete active herbal compound-target-pathway-biomarker network to explain the therapeutic efficacy of FA toward FD (Figure 3(f)) (Supplementary Material S4).

3.8. Experimental Validation. Fc epsilon RI signaling pathway is an activation pathway for mast cells [32]. From our observations, mast cells aggregated and degranulation rates were increased in the FD group, while FA intervention attenuated these phenomena (Figure 5(d)). To further validate the influence of Fc epsilon RI signaling in FD rats, we experimentally verified the hub target and its upstream and downstream proteins (tyrosine-protein kinase (Lyn), spleen tyrosine kinase (Syk), Mek, P-Mek, Erk, P-Erk1/2, MLCK, Mlc2, and P-Mlc2) using qPCR and western blotting. The P-Mek, P-Erk, MLCK, and P-Mlc2 protein levels were

significantly increased in model groups when compared with controls (Figure 5(a)). Western blot greyscale quantification P-Mek/Mek, P-Erk/Erk, P-Mlc2/Mlc2, and MLCK/β-actin analyses are shown ($P < 0.05$, $P < 0.01$, Figure 5(b)). P-Mek, P-Erk, MLCK, and P-Mlc2 expression decreased in the FA group when compared with the FD group ($P < 0.05$), while ZO-1 and occludin expression increased in the FA group when compared with the FD group ($P < 0.05$, $P < 0.01$, Figures 2(e), 2(h) and 2(i)). The mRNA expression of Lyn, Syk, Erk, and Mek was significantly increased in model groups when compared with controls ($P < 0.01$) and decreased in the FA group when compared with the FD group ($P < 0.01$, Figure 5(c)).

4. Discussion

FD is a chronic GI disorder characterized by motility disturbances and visceral hypersensitivity and requires long-term effective pharmacological treatment. FA is the dried
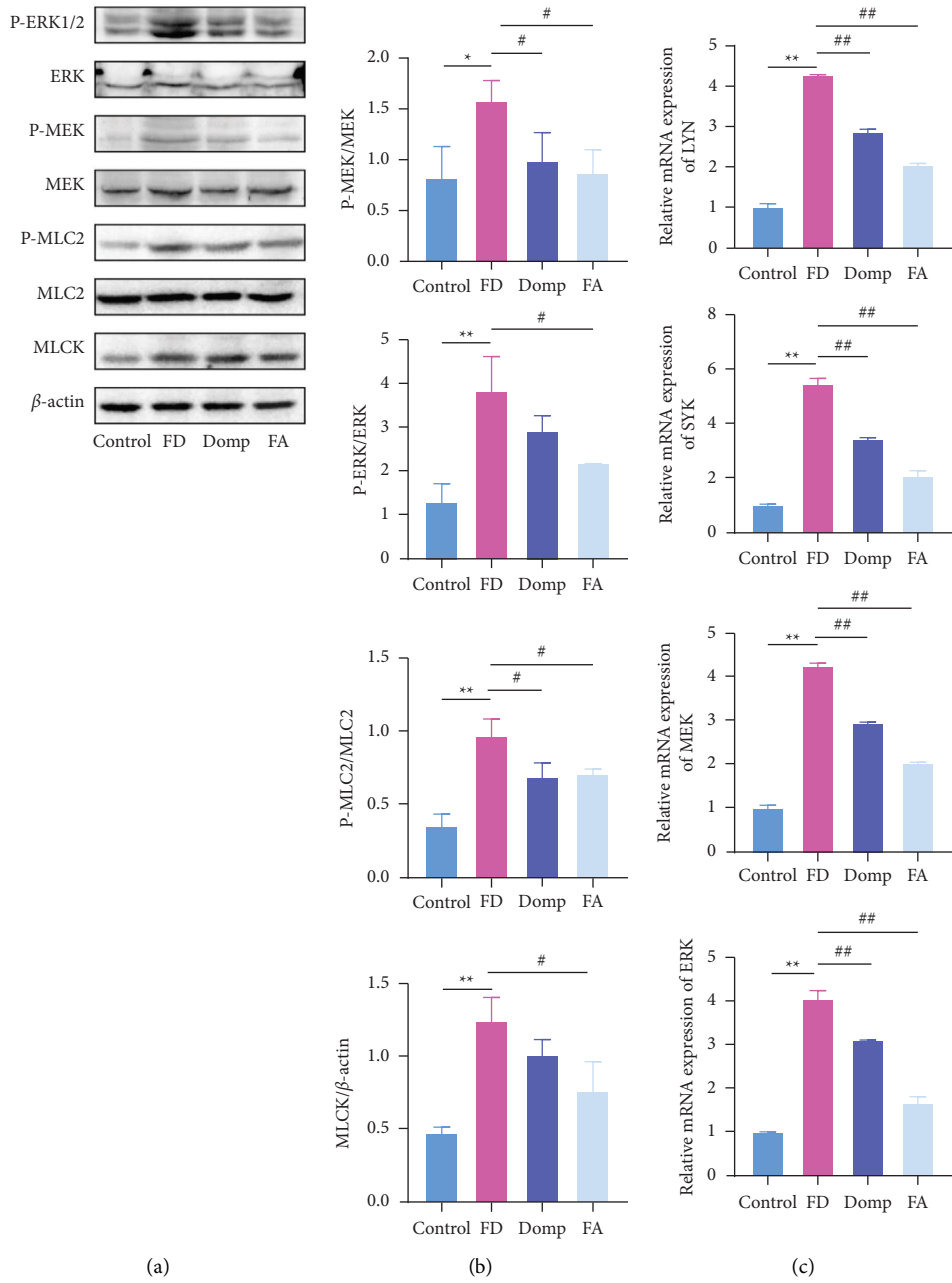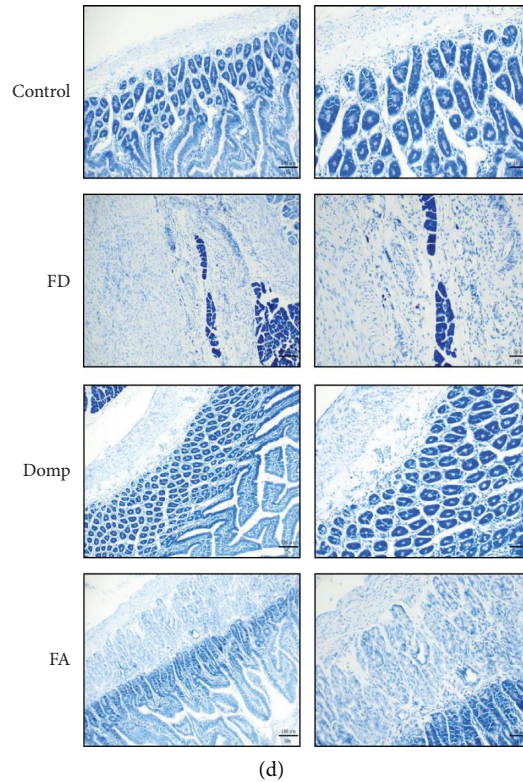
(a)

(b)

(c)

FIGURE 5: Continued.

(d)

Figure 5: Effect of FA on the Fc epsilon RI signal pathway. (a) Representative images of P-Erk1/2, Erk, P-Mek, Mek, P-Mlc2, Mlc2, and Mlck. (b) P-Erk1/2, P-Mek, P-Mlc2, and MLCK protein expressions ($n = 3$). (c) Relative mRNA expression of Erk, Mek, Lyn, and Syk ($n = 3$). (d) Representative images for mast cell stained with toluidine blue solution (scar bars: $100\,\mu$m, $200\,\mu$m). Values are presented as the means $\pm$ SD. $^{*}P < 0.05$ and $^{**}P < 0.01$ were compared with the control group. $^{\#}P < 0.05$ and $^{\#\#}P < 0.01$ were compared with the FD group.

unripe fruit of *Citrus aurantium* L. and its cultivated varieties, and it is a medicinal and edible fruit whose potential therapeutic effects reduce inflammation and promote GI motility [33, 34]. These key factors encouraged us to investigate the underlying FA mechanisms toward ameliorating FD. We confirmed these effects and demonstrated that anti-FD mechanisms were closely linked to mast cell-induced inflammatory responses. These findings facilitated the construction of a comprehensive network which improved our understanding of several interrelated FA mechanisms in improving FD in an IA-induced rat model.

Rats in the IA-induced FD group had dull hair, slow weight gain, low food intake, impaired GI motility, and prolonged GI emptying time. After FA administration, the FD disease status improved to some extent. Also, inflammatory cell infiltration in the local mucosa of FD rat groups was observed in pathological sections, while no infiltration was observed in the FA group. Growing evidence now suggests a role for intestinal epithelial barrier disruption and inflammation in FD [35, 36]. Changes in TJ proteins disrupt the intestinal epithelial barrier, which allows microorganisms in the intestinal lumen to promote abnormal immune responses, with excessive bacterial antigen leakage from the mucosa gradually degrading TJs [37, 38]. TNF-α impairs intestinal barriers by inducing apoptosis in epithelial cells and altering TJ structure and function [37], while IL-1β increases TJ permeability in human intestinal epithelial cells

[38]. In our study, TNF-α and IL-1β levels were elevated in the FD group, while the FA intervention down-regulated their secretion. Also, ZO-1 and occludin were down-regulated in the FD group, while this was reversed in the FA group. TJ defects may facilitate the passage of dietary antigens and bacterial products through the epithelial barrier, where they enter the lamina propria and possibly induce inflammatory changes [39]. Therefore, we confirmed the therapeutic potential of FA as it restored epithelial barrier structure and function to alleviate the effects of FD.

To further explore mechanisms whereby FA generates anti-inflammation and repairing intestinal barrier properties, we performed an integrated study on each rat group by combining metabolomics and systemic pharmacology approaches. First of all, we identified the FA extract through UPLC-QTOF-MS/MS technology, screened the active components, collected the targets for the identified components through OB and DL, collected the disease targets according to the disease database of FD, and obtained the key targets of systemic pharmacology through interactive analysis. Then, we analyzed the differential metabolite through metabolomics technology, integrated the differential metabolite and key target, and obtained the core pathway. Biomarker is able to participate in the regulation of core pathway. Finally, we established an active herbal compound-target-pathway-biomarker network. Through the above analysis, we targeted Fc epsilon RI signaling
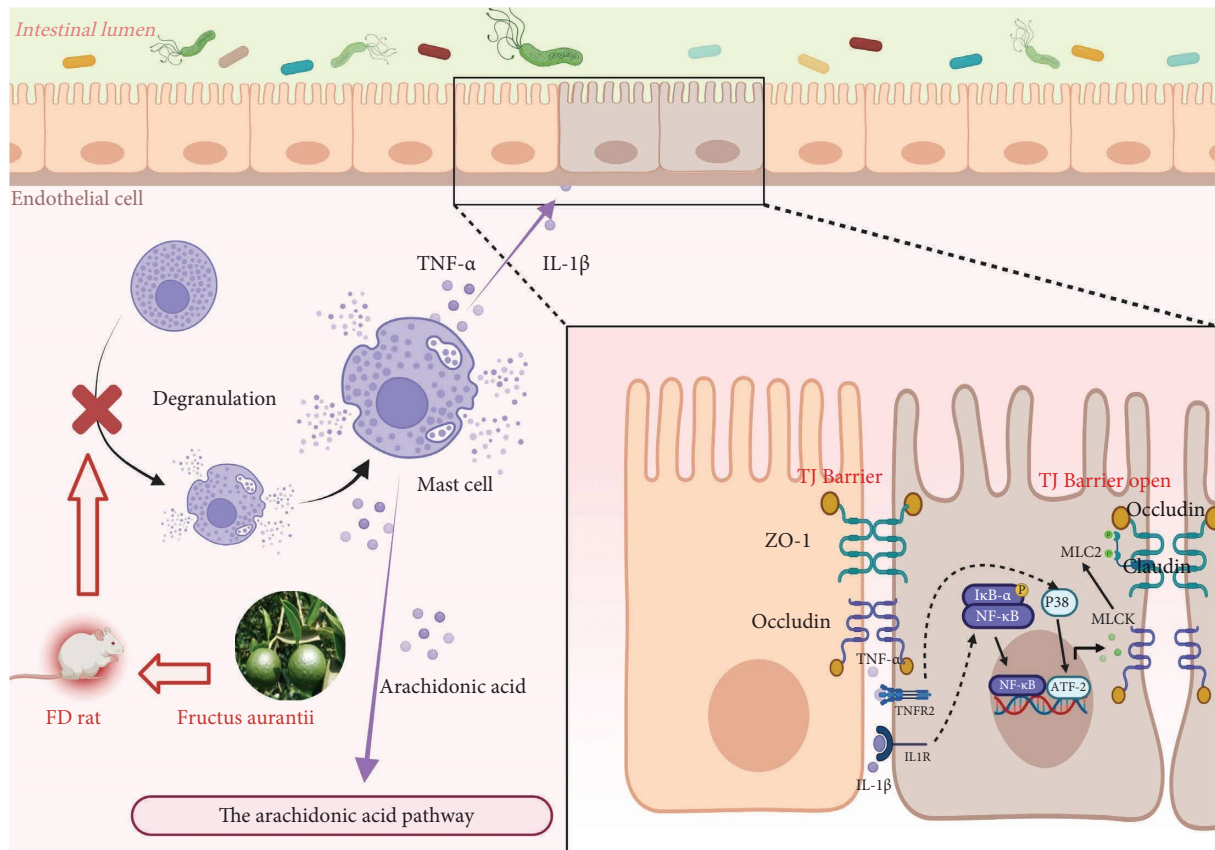
FIGURE 6: The molecular mechanisms of FA in treating FD (created with Biorender.com) FA reversed IA-induced FD in rats by regulating Fc epsilon RI signaling pathway to interfere with mast cell degranulation. FA treatment reduced mast cell activation and degranulation, decreased IL-1β and TNF-α secretion, and attenuated arachidonic acid pathway activation. In addition, it downregulated the expression of ZO-1 and occludin by reducing the phosphorylation of MLC2. It repaired the intestinal barrier, prevented the luminal antigen passing through the epithelial cells, and induced inflammatory reaction. ($\longrightarrow$ direct action, $\cdots\cdots\triangleright$ indirect action, and pathogenic antigen).

pathway, which is a mast cell activation pathway, and downstream arachidonic acid metabolism as further experimental verification pathways.

Mast cell infiltration and ultrastructural changes are reported in the duodena of FD patients, and such infiltration may be associated with chronic stress, intestinal flora, and acid hypersensitivity [40–42]. Thus, mast cell activation may be the pathological basis of mild intestinal inflammation in FD [31, 43]. Mast cell activation relies on several complex signal transduction steps; the main Src family kinase involved in these initial stages is Lyn [44]. When tyrosine residues in FceRI b and c chains are phosphorylated by Lyn, the phosphorylated immunoreceptor tyrosine-based activation motif of FceRI b and c chains provided the SH2 domain of Syk with high-affinity docking sites [45]. As the initial signaling molecule for mast cell activation, Syk regulates the phosphorylation of its downstream Mek, which phosphorylates both serine/threonine and tyrosine residues in Erk1/2, triggering its activation and subsequent cytosolic and nuclear activity. Erk1/2 is activated by MAPKs, which causes the nuclear translocation of AP-1, its transcription, and cytokine production, including IL-1β and TNF-α. Syk inhibition also leads to the downstream inhibition of MAPK,

Mek, and Erk, suggesting a role in disease initiation and progression [46–48]. Mast cell degranulation releases TNF-α, IL-1β, and arachidonic acid metabolites. TNF-α and IL-1β bind to TNFR2 and IL-1R on intestinal epithelial cell surfaces to activate P38 and NF-κB, thereby inducing the transcription and enzyme activation of MLCK [49]. MLCK is a specific substrate enzyme of Mlc2 and specifically phosphorylates Ser18 and Thr19 residues in Mlc2. Then, p-Mlc2 activates the ATPase domain of the myosin heavy chain head, producing energy which causes cytoskeletal actin filaments to slide [50]. This causes the cell membrane endocytosis of TJ proteins and other transmembrane proteins (including occludin and ZO-1), which hinder TJ proteins in forming gaps, ultimately increasing epithelial permeability [51] and intestinal barrier disruption. Conversely, impaired barrier function may also lead to low-grade inflammation, as animal models showed that inflammation is weakened after increased intestinal permeability [52]. Arachidonic acid is also an important inflammatory mediator; it participates in and promotes inflammatory responses [53]. Many studies have reported that elevated levels of bodily arachidonic acid are closely associated with many diseases, including inflammatory bowel disease, arthritis,

and stroke [54–56]. We showed that arachidonic acid levels increased in FD animals but decreased in the FA group, suggesting that FA blocked inflammation by regulating arachidonic acid metabolism (Figure 6).

In conclusion, FA reversed IA-induced FD in rats by regulating Fc epsilon RI signaling pathway to interfere with mast cell degranulation. FA treatment lowered Lyn and Syk expression, down-regulated Mek and Erk phosphorylation, reduced mast cell activation and degranulation, decreased IL-1β and TNF-α secretion, and attenuated arachidonic acid pathway activation, thereby reducing the IL-1β and TNF-α induced downregulation of intestinal epithelial TJ proteins (ZO-1 and Occludin). Physiologically, these molecular events ultimately ameliorated IA-induced intestinal barrier function disruption and duodenal inflammation.

5. Conclusions

In the present study, an integrative metabolomics, and systematic pharmacology-based strategy was proposed to uncover the material basis and mechanisms of FA in treating FD. A total of 54 potential biomarkers and 252 targets related to 20 pathways were clarified, and 38 components of FA were identified. Then, we verified that FA can activate mast cells to treat FD through Fc epsilon RI signaling pathway. In short, we generated a new biochemical and molecular paradigm for FA actions against FD, these results confirm that FA has the potential to ameliorate FD. All our results also serve to explain the success of FA treatment of FD in humans in traditional Chinese medicine practice. This article only verified the molecular mechanism of FA in treating FD from Fc epsilon RI signaling pathway. Whether FA plays a role through other signaling pathways needs to be further studied. We hope it can be improved in the follow-up study.

Data Availability

The data used to support the findings of this study are available within the article and additional information can be obtained from the corresponding author upon request.

Conflicts of Interest

The authors declare no conflicts of interest.

Authors' Contributions

Sicong Liu conceptualized the study; Tianjiao Li, Bing Qi, and Ying Meng developed the methodology; Yongrui Bao administered the project; Sicong Liu, Ying Zheng, Yi Zheng, and Xi Luo visualized the study; Sicong Liu wrote the original draft; Xiansheng Meng, Yongrui Bao, Shuai Wang, and Jiapeng Leng wrote, reviewed, and edited. Xiansheng Meng carried out the funding acquisition. All authors revised the manuscript and approved the final version.

Acknowledgments

Supplementary Materials

Supplementary Materials S1: Calculation of dosage; Supplementary Materials S2: Nutritious semisolid paste containing graphite powder; Supplementary Materials S3: Information about differential metabolites; Supplementary Materials S4: Herb-activecompound-hub target-pathway-biomarkers network; Supplementary Materials S5: Metabolite enrichment pathways. (*Supplementary Materials*)

References

[1] D. A. Drossman and W. L. Hasler, "Rome IV-functional GI disorders: disorders of gut-brain interaction," *Gastroenterology*, vol. 150, no. 6, pp. 1257–1261, 2016.

[2] J. Tack, N. J. Talley, M. Camilleri et al., "Functional gastro-duodenal disorders," *Gastroenterology*, vol. 130, no. 5, pp. 1466–1479, 2006.

[3] S. Liu, S. I. Hagiwara, and A. Bhargava, "Early-life adversity, epigenetics, and visceral hypersensitivity," *Neuro-Gastroenterology and Motility*, vol. 29, no. 9, Article ID e13170, 2017.

[4] H. Vanheel and R. Farré, "Changes in gastrointestinal tract function and structure in functional dyspepsia," *Nature Reviews Gastroenterology & Hepatology*, vol. 10, no. 3, pp. 142–149, 2013.

[5] H. Vanheel, M. Vicario, T. Vanuytsel et al., "Impaired duodenal mucosal integrity and low-grade inflammation in functional dyspepsia," *Gut*, vol. 63, no. 2, pp. 262–271, 2014.

[6] L. Ohman and M. Simrén, "Pathogenesis of IBS: role of inflammation, immunity and neuroimmune interactions," *Nature Reviews Gastroenterology & Hepatology*, vol. 7, no. 3, pp. 163–173, 2010.

[7] K. Mönkemüller and P. Malfertheiner, "Drug treatment of functional dyspepsia," *World Journal of Gastroenterology*, vol. 12, no. 17, pp. 2694–2700, 2006.

[8] H. Wu, Z. Jing, X. Tang et al., "To compare the efficacy of two kinds of Zhizhu pills in the treatment of functional dyspepsia of spleen-deficiency and qi-stagnation syndrome: a randomized group sequential comparative trial," *BMC Gastroenterology*, vol. 11, no. 1, p. 81, 2011.

[9] Z. R. Xu, C. H. Jiang, S. Y. Fan, R. Yan, N. Xie, and C. Wu, "Comparative pharmacokinetics of naringin and neo-hesperidin after oral administration of flavonoid glycosides from Aurantii Fructus Immaturus in normal and gastrointestinal motility disorders mice," *Chinese Herbal Medicines*, vol. 11, no. 3, pp. 314–320, 2019.

[10] Y. Yang, Z. Ding, R. Zhong et al., "Cardioprotective effects of a Fructus Aurantii polysaccharide in isoproterenol-induced myocardial ischemic rats," *International Journal of Biological Macromolecules*, vol. 155, pp. 995–1002, 2020.

[11] Y. J. Zhang, W. Huang, X. Huang et al., "Fructus Aurantii induced antidepressant effect via its monoaminergic mechanism and prokinetic action in rat," *Phytomedicine*, vol. 19, no. 12, pp. 1101–1107, 2012.

[12] X. Li, Q. Liang, Y. Sun et al., "Potential mechanisms responsible for the antinephrolithic effects of an aqueous extract of Fructus aurantii," *Evidence-based Complementary and Alternative Medicine*, vol. 2015, Article ID 491409, 11 pages, 2015.

[13] J. Ni, Y. Guo, N. Chang et al., "Effect of N-methyltyramine on the regulation of adrenergic receptors via enzymatic epinephrine synthesis for the treatment of gastrointestinal disorders," *Biomedicine & Pharmacotherapy*, vol. 111, pp. 1393–1398, 2019.

[14] X. Y. Qu, S. N. Li, and Z. W. Sun, "Analysis of the relationship between the chemical components of Fructus Aurantii Aurantii immaturus and the treatment of functional dyspepsia and experimental verification," *Chinese Herbal Medicines*, vol. 53, no. 20, pp. 6521–6528, 2022.

[15] S. K. Ha, H. Y. Park, H. Eom, Y. Kim, and I. Choi, "Narirutin fraction from citrus peels attenuates LPS-stimulated inflammatory response through inhibition of NF-κB and MAPKs activation," *Food and Chemical Toxicology*, vol. 50, no. 10, pp. 3498–3504, 2012.

[16] H. Cao, J. Liu, P. Shen et al., "Protective effect of naringin on DSS-induced ulcerative colitis in mice," *Journal of Agricultural and Food Chemistry*, vol. 66, no. 50, pp. 13133–13140, 2018.

[17] F. Wang, C. Zhao, G. Tian et al., "Naringin alleviates atherosclerosis in ApoE-/- mice by regulating cholesterol metabolism involved in gut microbiota remodeling," *Journal of Agricultural and Food Chemistry*, vol. 68, no. 45, pp. 12651–12660, 2020.

[18] C. B. Newgard, "Metabolomics and metabolic diseases: where do we stand?" *Cell Metabolism*, vol. 25, no. 1, pp. 43–56, 2017.

[19] A. H. Zhang, Z. M. Ma, L. Kong et al., "High-throughput lipidomics analysis to discover lipid biomarkers and profiles as potential targets for evaluating efficacy of Kai-Xin-San against APP/PS1 transgenic mice based on UPLC-Q/TOF-MS," *Biomedical Chromatography: Biomedical Chromatography*, vol. 34, no. 2, p. e4724, 2020.

[20] C. Hu and G. Xu, "Metabolomics and traditional Chinese medicine," *TRAC Trends in Analytical Chemistry*, vol. 61, pp. 207–214, 2014.

[21] A. L. Hopkins, "Network pharmacology," *Nature Biotechnology*, vol. 25, no. 10, pp. 1110-1111, 2007.

[22] A. L. Hopkins, "Network pharmacology: the next paradigm in drug discovery," *Nature Chemical Biology*, vol. 4, no. 11, pp. 682–690, 2008.

[23] J. Han, M. Wan, Z. Ma, C. Hu, and H. Yi, "Prediction of targets of curculigoside A in osteoporosis and rheumatoid arthritis using network pharmacology and experimental verification," *Drug Design, Development and Therapy*, vol. 14, pp. 5235–5250, 2020.

[24] W. Xia, S. Hu, M. Wang, F. Xu, L. Han, and D. Peng, "Exploration of the potential mechanism of the Tao Hong Si Wu Decoction for the treatment of postpartum blood stasis based on network pharmacology and in vivo experimental verification," *Journal of Ethnopharmacology*, vol. 268, Article ID 113641, 2021.

[25] F. X. Zhang, Z. T. Li, X. Yang, Z. Xie, and Y. Dai, "Discovery of anti-flu substances and mechanism of Shuang-Huang-Lian water extract based on serum pharmaco-chemistry and network pharmacology," *Journal of Ethnopharmacology*, vol. 268, Article ID 113660, 2021.

[26] X. S. Meng, *Modern Research and Practice of Qizhiweitong Formula*, People's Medical Publishing House, Beijing, China, 2018.

[27] L. S. Liu, J. H. Winston, M. M. Shenoy, G. Song, J. D. Chen, and P. J. Pasricha, "A rat model of chronic gastric sensorimotor dysfunction resulting from transient neonatal gastric irritation," *Gastroenterology*, vol. 134, no. 7, pp. 2070–2079, 2008.

[28] J. Wang, T. Zhang, C. J. Johnston et al., "Protein thiol oxidation in the rat lung following e-cigarette exposure," *Redox Biology*, vol. 37, Article ID 101758, 2020.

[29] N. S. Harhaj and D. A. Antonetti, "Regulation of tight junctions and loss of barrier function in pathophysiology," *The International Journal of Biochemistry & Cell Biology*, vol. 36, no. 7, pp. 1206–1237, 2004.

[30] J. König, J. Wells, P. D. Cani et al., "Human intestinal barrier function in health and disease," *Clinical and Translational Gastroenterology*, vol. 7, no. 10, p. e196, 2016.

[31] S. Shi, H. Yan, Y. Chen et al., "Pharmacokinetic study of precisely representative antidepressant, prokinetic, anti-inflammatory and anti-oxidative compounds from Fructus aurantii and Magnolia Bark," *Chemico-Biological Interactions*, vol. 315, Article ID 108851, 2020.

[32] V. Hernandez-Hansen, A. J. Smith, Z. Surviladze et al., "Dysregulated FcεRI signaling and altered fyn and SHIP activities in lyn-deficient mast cells," *The Journal of Immunology*, vol. 173, no. 1, pp. 100–112, 2004.

[33] J. Q. Feng, J. F. Song, and S. Q. Zhao, "Study on the spectral effect of flavonoids in Fructus aurantii in regulating gastrointestinal motility," *Chinese Journal of Modern Applied Pharmacy*, vol. 39, no. 17, pp. 2241–2245, 2022.

[34] S. Lechuga and A. I. Ivanov, "Disruption of the epithelial barrier during intestinal inflammation: quest for new molecules and mechanisms," *Biochimica et Biophysica Acta (BBA) - Molecular Cell Research*, vol. 1864, no. 7, pp. 1183–1194, 2017.

[35] P. Wu, W. D. Jiang, J. Jiang et al., "Dietary choline deficiency and excess induced intestinal inflammation and alteration of intestinal tight junction protein transcription potentially by modulating NF-κB, STAT and p38 MAPK signaling molecules in juvenile Jian carp," *Fish & Shellfish Immunology*, vol. 58, pp. 462–473, 2016.

[36] M. Schumann, D. Günzel, N. Buergel et al., "Cell polarity-determining proteins Par-3 and PP-1 are involved in epithelial tight junction defects in coeliac disease," *Gut*, vol. 61, no. 2, pp. 220–228, 2012.

[37] T. Suzuki, "Regulation of intestinal epithelial permeability by tight junctions," *Cellular and Molecular Life Sciences*, vol. 70, no. 4, pp. 631–659, 2013.

[38] A. Fischer, M. Gluth, U. F. Pape, B. Wiedenmann, F. Theuring, and D. C. Baumgart, "Adalimumab prevents barrier dysfunction and antagonizes distinct effects of TNF-α on tight junction proteins and signaling pathways in intestinal epithelial cells," *American Journal of Physiology - Gastrointestinal and Liver Physiology*, vol. 304, no. 11, pp. G970–G979, 2013.

[39] J. Santos, M. Benjamin, P. C. Yang, T. Prior, and M. H. Perdue, "Chronic stress impairs rat growth and jejunal epithelial barrier function: role of mast cells," *American*

Journal of Physiology - Gastrointestinal and Liver Physiology, vol. 278, no. 6, pp. G847–G854, 2000.

[40] J. Gao, T. Xiong, G. Grabauskas, and C. Owyang, "Mucosal serotonin reuptake transporter expression in irritable bowel syndrome is modulated by gut microbiota via mast cell-prostaglandin E2," *Gastroenterology*, vol. 162, no. 7, pp. 1962–1974.e6, 2022.

[41] G. Sarnelli, M. Pesce, L. Seguella et al., "Impaired duodenal palmitoyl- ethanolamide release underlies acid-induced mast cell activation in functional dyspepsia," *Cellular and Molecular Gastroenterology and Hepatology*, vol. 11, no. 3, pp. 841–855, 2021.

[42] H. Vanheel, M. Vicario, W. Boesmans et al., "Activation of eosinophils and mast cells in functional dyspepsia: an ultrastructural evaluation," *Scientific Reports*, vol. 8, no. 1, p. 5383, 2018.

[43] S. Kraft and J. P. Kinet, "New developments in FcεRI regulation, function and inhibition," *Nature Reviews Immunology*, vol. 7, no. 5, pp. 365–378, 2007.

[44] P. Draber, I. Halova, F. Levi-Schaffer, and L. Draberova, "Transmembrane adaptor proteins in the high-affinity IgE receptor signaling," *Frontiers in Immunology*, vol. 2, p. 95, 2011.

[45] E. M. Corr, C. C. Cunningham, and A. Dunne, "Cholesterol crystals activate Syk and PI3 kinase in human macrophages and dendritic cells," *Atherosclerosis*, vol. 251, pp. 197–205, 2016.

[46] R. O. de Castro, "Regulation and function of syk tyrosine kinase in mast cell signaling and beyond," *Journal of Signal Transduction*, vol. 2011, Article ID 507291, 507299 pages, 2011.

[47] F. Berenbaum, L. Humbert, G. Bereziat, and S. Thirion, "Concomitant recruitment of ERK1/2 and p38 MAPK signalling pathway is required for activation of cytoplasmic phospholipase A2 via ATP in articular chondrocytes," *Journal of Biological Chemistry*, vol. 278, no. 16, pp. 13680–13687, 2003.

[48] L. Su, S. C. Nalle, L. Shen et al., "TNFR2 activates MLCK-dependent tight junction dysregulation to cause apoptosis-mediated barrier loss and experimental colitis," *Gastroenterology*, vol. 145, no. 2, pp. 407–415, 2013.

[49] M. G. Laukoetter, M. Bruewer, and A. Nusrat, "Regulation of the intestinal epithelial barrier by the apical junctional complex," *Current Opinion in Gastroenterology*, vol. 22, no. 2, pp. 85–89, 2006.

[50] D. Ye and T. Y. Ma, "Cellular and molecular mechanisms that mediate basal and tumour necrosis factor-alpha-induced regulation of myosin light chain kinase gene activity," *Journal of Cellular and Molecular Medicine*, vol. 12, no. 4, pp. 1331–1346, 2008.

[51] M. C. Arrieta, K. Madsen, J. Doyle, and J. Meddings, "Reducing small intestinal permeability attenuates colitis in the IL10 gene-deficient mouse," *Gut*, vol. 58, no. 1, pp. 41–48, 2009.

[52] M. Hoxha, "A systematic review on the role of eicosanoid pathways in rheumatoid arthritis," *Advances in Medical Sciences*, vol. 63, no. 1, pp. 22–29, 2018.

[53] H. K. Chung, Y. Cho, H. J. Do, K. Oh, W. K. Seo, and M. J. Shin, "Plasma phospholipid arachidonic acid and lignoceric acid are associated with the risk of cardioembolic stroke," *Nutrition Research*, vol. 35, no. 11, pp. 1001–1008, 2015.

[54] M. Urbini, V. Petito, F. de Notaristefani, F. Scaldaferri, A. Gasbarrini, and L. Tortora, "ToF-SIMS and principal component analysis of lipids and amino acids from inflamed and dysplastic human colonic mucosa," *Analytical and Bioanalytical Chemistry*, vol. 409, no. 26, pp. 6097–6111, 2017.

[55] W. Wang, L. Zhao, Z. He et al., "Metabolomics-based evidence of the hypoglycemic effect of Ge-Gen-Jiao-Tai-Wan in type 2 diabetic rats via UHPLC-QTOF/MS analysis," *Journal of Ethnopharmacology*, vol. 219, pp. 299–318, 2018.

[56] Z. Yuan, L. Yang, X. Zhang, P. Ji, and Y. Wei, "Therapeutic effect of n-butanol fraction of Huang-lian-Jie-du Decoction on ulcerative colitis and its regulation on intestinal flora in colitis mice," *Biomedicine & Pharmacotherapy*, vol. 121, Article ID 109638, 2020.